

## Efficient perturbation-tracking method for directly probing the spectral phonon properties from molecular dynamics simulations

Zexi Zheng<sup>1,\*</sup>, Yang Li<sup>1</sup>, Xiang Chen<sup>2</sup> and Youping Chen<sup>1</sup>

<sup>1</sup>Department of Mechanical and Aerospace Engineering, University of Florida, Gainesville, Florida 32611, USA

<sup>2</sup>Institute for Micromanufacturing, Mechanical Engineering, Louisiana Tech University, Ruston, Louisiana 71272, USA



(Received 20 August 2020; accepted 1 November 2020; published 19 November 2020)

Existing methods for directly extracting the spectral phonon properties from molecular dynamics (MD) simulations, like the normal mode analysis (NMA) and spectral energy density analysis, all require a very long simulation time to produce reliable results with good convergence. So far, these methods are mainly applied in studies using small systems and with empirical potentials, as the heavy computational load has greatly hindered their further applications. Here we propose a perturbation-tracking (PT) method for directly probing the mode-wise phonon anharmonic frequencies and lifetimes. We show that results obtained from our method are in excellent agreement with those from the conventional NMA approach, using Si as the model material system. Comparing with the NMA approach, the PT method offers a greater accuracy and significant improvement of efficiency. It takes an average of two orders of magnitude and up to three orders of magnitude less simulation time to obtain the same lifetime result of a phonon mode with intermediate to high accuracy. Meanwhile, our method preserves all the dynamics of probed phonon mode from a particular state, which means it is capable of studying the transient thermal transport processes in a nonequilibrium system. Besides the exceptional efficiency, our method also comes with freedom to choose to probe only those modes of interest. This makes it ideal for use with large systems and in computationally demanding applications, such as *ab initio* MD simulations. Moreover, the PT method we propose here is very straightforward and easy to implement.

DOI: [10.1103/PhysRevE.102.053311](https://doi.org/10.1103/PhysRevE.102.053311)

### I. INTRODUCTION

Much attention has been given to the search of novel materials and structures with desired thermal transport properties [1–3]. The thermal conductivity is closely related to the properties of phonons, which are the dominant heat carriers in semiconductors and dielectrics. In order to correctly interpret measured thermal conductivity results from experiments and to seek a deeper understanding of the underlying mechanisms, gaining insight into the spectral transport properties of phonons has become a necessity [4–7].

Based on the Boltzmann transport equation (BTE) under the relaxation time approximation (RTA), the lattice thermal conductivity  $\kappa$  can be written in terms of the spectral phonon lifetime (which is also called relaxation time or scattering time)  $\tau$ , the specific heat  $c$ , and the group velocity  $\bar{v}$  as

$$\kappa_{\mu} = \frac{1}{V} \sum_{\lambda} \tau_{\lambda} c_{\lambda} (\bar{v}_{\lambda} \cdot \bar{e}_{\mu})^2, \quad (1)$$

where  $V$  is the system volume and  $\bar{e}_{\mu}$  is a unit vector along the transport direction  $\mu$ . The summation runs over all available phonon modes  $\lambda \equiv (\vec{k}, \nu)$  with wave vector  $\vec{k}$  and polarization  $\nu$ . The product of the group velocity and lifetime gives the phonon mean free path, which is extensively used to explain different thermal transport phenomena such as the size

effects. Two of the three key ingredients, the mode specific heat and the group velocity can be readily calculated once the phonon dispersion relations are known. To obtain the anharmonic vibrational frequencies is challenging but necessary for improving the accuracy when calculating  $\kappa$  at a finite temperature. The remaining difficulty is to accurately and efficiently determine the spectral phonon lifetimes.

Methodologies for predicting phonon properties and the lattice thermal conductivity have been under active development in two main categories: anharmonic lattice dynamics (ALD) calculations and molecular dynamics (MD) simulations. Since the third-order ALD method was first proposed to calculate the intrinsic three-phonon scattering rates via Fermi's golden rule, calculations based on ALD have been carried out to predict phonon lifetimes from density functional theory (DFT) [8,9] and combined with BTE to predict the lattice thermal conductivity [10,11]. The ALD approach with interatomic force constants determined from first principles or from an empirical potential is now widely employed [4,5,12]. However, there are certain limitations associated with ALD calculations. For instance, the approach is based on perturbation theory, which gives accurate results at a relatively low temperature. But it may fail at high temperatures or in strongly anharmonic systems [13,14], given that only three-phonon or at most four-phonon processes are considered [15–17].

Approaches based on molecular dynamics (MD) simulations on the other hand have advantages over ALD calculations at high temperatures since full orders of anharmonicity are naturally incorporated. Other issues related to

\*Corresponding author: zexizheng@outlook.com

anharmonic effects, such as imaginary phonon frequencies solved from lattice dynamics calculations [14,18], can also be easily handled through MD simulations at a finite temperature [19]. Anharmonic phonon frequencies have been determined either indirectly by solving the dynamical matrix with force constants obtained from an MD simulation or directly through Fourier analysis of the statistical result from a simulation run. For the indirect approach, Kong proposed a Green’s function method to construct the dynamical matrix based on the fluctuation-dissipation theorem [20]. Hellman *et al.* developed a temperature-dependent effective potential (TDEP) method [19,21] to subsume anharmonic effects in the effective force constants. The TDEP method was applied in *ab initio* molecular dynamics (AIMD) due to its efficiency. For the direct approach, the two most commonly adopted methods are the time domain normal mode analysis (NMA) [22–24] and the spectral energy density (SED) analysis [25–28]. Both the anharmonic phonon frequencies and phonon lifetimes can be extracted using either one of the two methods, which are basically equivalent [28,29]. In the time domain NMA, a time history of the normal mode amplitudes or mode energy is obtained by projecting the atomic trajectories onto each phonon mode in a system. The phonon lifetime of each mode is extracted by fitting the autocorrelation result to an exponential decay curve. If only the potential energy is used, the autocorrelation function gives a decay curve with oscillations, from which the anharmonic phonon frequency can be extracted. In the SED analysis, the kinetic energy of a single phonon mode or multiple modes with the same wave vector is calculated in the frequency domain through Fourier transform. The resulting time average gives a Lorentzian function for each phonon mode with its peak position as the frequency and full width at half maximum as inverse of the phonon lifetime. There are other MD simulation techniques and schemes for predicting lattice thermal conductivities such as the approach-to-equilibrium method [30–32], Green-Kubo method [33–36], and the direct method [37–40], which are more general and capable of dealing with complex material systems. Meanwhile, theories were developed for spectral decomposition of the heat flux for quantifying the contribution from various vibrational modes towards the total thermal conductivity [41,42]. In this work, we will limit our scope to the BTE-based phonon quasi-particle picture and only focus on getting the key phonon properties from MD simulations.

Most of the MD simulation studies for direct extraction of the spectral phonon properties especially those involving phonon lifetimes have been conducted using empirical potentials because of the high computational cost. Existing methods, whether based on autocorrelation function or SED, all require a long simulation time—usually hundreds of picoseconds to several nanoseconds—to produce reliable results with good convergence. This has greatly limited their applications in AIMD simulations. As a trade-off, the system size has to be very small [25,43,44], which often causes strong size effects that result in underestimation of the thermal conductivity. It is possible to accelerate the convergence process and improve result fitting from additional theoretical approaches [45], but it can be quite complicated and difficult to implement. Meanwhile, the reduction in the required simulation time is still limited as the auxiliary calculations do

not change the method itself. Moreover, for methods that rely on averaging to suppress the background noise from thermal fluctuations, the final result essentially reflects the overall statistical average and individual phonon processes on small timescales have all been washed away.

In this work, we propose a perturbation-tracking (PT) method to directly extract the spectral phonon properties from MD simulations. Unlike the statistics-based NMA or SED analysis, our method preserves all the dynamics of a decay process and offers great flexibility and exceptionally high efficiency for studying individual phonon modes of interest. The remaining article is structured as follows: In Sec. II, we introduce the PT method along with its theoretical background. Results from the PT method versus those from the time-domain NMA for the model material system Si are presented in Sec. III. We demonstrate the validity of the PT method for extracting anharmonic vibrational frequencies and phonon lifetimes, and provide detailed comparisons between the two methods on accuracy and efficiency. In Sec. IV, we further discuss the advantages, limitations, and application scenarios of the PT method. Section V ends with a summary and conclusions.

**II. THEORETICAL BACKGROUND AND METHOD**

Starting from lattice dynamics, the general equation of a traveling wave in a crystal can be written as

$$\begin{aligned} \vec{u}_\lambda \left( \begin{matrix} jl \\ t \end{matrix} \right) &= \frac{1}{\sqrt{m(j)}} A_\lambda \vec{\epsilon}_\lambda(j) \\ &\times \exp\{i[\vec{k} \cdot \vec{r}(jl) + \varphi_\lambda - \omega_\lambda t]\}, \end{aligned} \quad (2)$$

where  $\vec{u}_\lambda(jl, t)$  is the time-dependent displacement of atom  $j$  in the unit cell  $l$  under the influence of a vibrational mode  $\lambda$ ,  $A$  is the wave amplitude factor,  $m$  is the atomic mass,  $\vec{r}$  is the equilibrium position,  $\varphi$  is the relative phase,  $\omega$  is the angular frequency, and  $\vec{\epsilon}$  is the displacement vector. The angular frequency and the displacement vector are obtained by solving the eigenvalue problem,  $\omega_\lambda^2 \vec{\epsilon}_\lambda = \bar{D}(\vec{k}) \vec{\epsilon}_\lambda$ , with  $\bar{D}$  being the dynamical matrix. Within the harmonic approximation, the total displacement is a linear superposition of all available waves of different phonon modes as

$$\vec{u} \left( \begin{matrix} jl \\ t \end{matrix} \right) = \sum_\lambda \vec{u}_\lambda \left( \begin{matrix} jl \\ t \end{matrix} \right). \quad (3)$$

It is convenient to describe a lattice wave in reciprocal space by using the normal mode coordinate (NMC), which can be calculated from

$$Q_\lambda(t) = \sum_{jl} \sqrt{\frac{m(j)}{N}} \exp[-i\vec{k} \cdot \vec{r}(jl)] \vec{\epsilon}_\lambda^*(j) \cdot \vec{u} \left( \begin{matrix} jl \\ t \end{matrix} \right), \quad (4)$$

where  $N$  is the number of lattice points and the asterisk superscript denotes the complex conjugate. For the harmonic wave of a phonon normal mode,  $Q$  oscillates over time as

$$Q_\lambda(t) = Q_\lambda(0) \exp[-i\omega_\lambda t]. \quad (5)$$

In the presence of lattice anharmonicity, anharmonic interactions dampen the oscillations, which is seen as spectral

line broadening, and cause frequencies to shift from their harmonic values. If the frequency shift and linewidth are relatively small, the time-dependent NMC can be reintroduced as

$$P_\lambda(t) = Q_\lambda(0) \exp\{-i[\omega_\lambda + \Delta_\lambda - i\Gamma_\lambda]t\}, \quad (6)$$

where  $\Delta$  is the frequency shift and  $\Gamma$  is the linewidth. The phonon lifetime and linewidth are related as

$$\tau_\lambda = (2\Gamma_\lambda)^{-1}. \quad (7)$$

The use of  $P$  is to distinguish from the measured  $Q$  at time  $t$  because Eq. (6) describes the evolution of a phonon state initially started from time 0 that decays over time. Nevertheless, phonons in each mode are not only being scattered to but also created from other modes. The population of a phonon mode, which is proportional to the mode's energy, fluctuates about a mean value due to multiple phonon processes. At thermodynamic equilibrium, the average mode energy is  $\langle E_\lambda \rangle = \hbar\omega_\lambda(n_\lambda + 1/2)$ , where  $\hbar$  is reduced Planck's constant and  $n$  is the average phonon occupation number, which follows Bose-Einstein statistics. In the classical limit or for a classical system, according to the equipartition theorem, it reduces to

$$\langle E_\lambda \rangle = k_B T, \quad (8)$$

where  $k_B$  is Boltzmann's constant. The simultaneous creation and annihilation of phonons at any moment gives a new state starting from that moment. Because  $Q$  measures the current, updated state, the time-dependent energy of a normal mode can be calculated as

$$E_\lambda(t) = V_\lambda(t) + K_\lambda(t) = \frac{1}{2}\omega_\lambda^2 Q_\lambda^*(t)Q_\lambda(t) + \frac{1}{2}\dot{Q}_\lambda^*(t)\dot{Q}_\lambda(t), \quad (9)$$

where  $V$  is the potential energy,  $K$  is the kinetic energy, and  $\dot{Q}$  is the time derivative of the NMC, which can be determined from atomic velocities  $\vec{u}$  similar to Eq. (4):

$$\dot{Q}_\lambda(t) = \sum_{jl} \sqrt{\frac{m(j)}{N}} \exp[-i\vec{k} \cdot \vec{r}(jl)] \vec{\epsilon}_\lambda^*(j) \cdot \vec{u}\left(\begin{matrix} jl \\ t \end{matrix}\right). \quad (10)$$

Since  $\langle V_\lambda \rangle = \langle K_\lambda \rangle$ , we have

$$\langle Q_\lambda^*(t)Q_\lambda(t) \rangle = \frac{k_B T}{\omega_\lambda^2}. \quad (11)$$

So the measured NMC sequence does not directly reflect the decay of a particular normal mode state as described by Eq. (6). In order to extract the effective decay rate of a normal mode, the common way has been using a statistical approach, such as the autocorrelation function (NMA) or SED analysis. The method we propose here is, on the other hand, using a different strategy.

The two NMCs, one in Eq. (4) that measures the current phonon state and the other in Eq. (6) that describes a previous decaying state are related as

$$Q_\lambda(t) = P_\lambda(t) + C_\lambda(t) = Q_\lambda(0) \exp(-i\omega_\lambda^A t) \exp(-\Gamma_\lambda t) + C_\lambda(t), \quad (12)$$

where  $\omega_\lambda^A = \omega_\lambda + \Delta_\lambda$  is the anharmonic angular frequency and  $C$  is a time-dependent complex number, introduced here as an accumulated change in the NMC due to the newly created phonons in mode  $\lambda$ . In order to reveal the oscillatory and decaying behavior of a damped mode, the effect from  $C$  needs to be eliminated. We introduce a perturbation  $\chi$  to the initial state of phonon mode  $\lambda$ :

$$Q_\lambda^p(0) = Q_\lambda(0) + \chi_\lambda, \quad (13)$$

where

$$\chi_\lambda = \sum_{jl} \sqrt{\frac{m(j)}{N}} \exp[-i\vec{k} \cdot \vec{r}(jl)] \vec{\epsilon}_\lambda^*(j) \cdot \vec{u}_\lambda^p(jl), \quad (14)$$

with

$$\vec{u}_\lambda^p(jl) = \frac{1}{\sqrt{m(j)}} A_\lambda^p \vec{\epsilon}_\lambda(j) \exp\{i[\vec{k} \cdot \vec{r}(jl) + \phi_\lambda^p]\}, \quad (15)$$

in which  $A_\lambda^p$  is the amplitude and  $\phi_\lambda^p$  is the relative phase of the perturbation in real space. The corresponding displacement field of the perturbed system at  $t = 0$  is then

$$\vec{u}^p\left(\begin{matrix} jl \\ 0 \end{matrix}\right) = \vec{u}\left(\begin{matrix} jl \\ 0 \end{matrix}\right) + \vec{u}_\lambda^p(jl), \quad (16)$$

and the velocity field is

$$\vec{u}^p\left(\begin{matrix} jl \\ 0 \end{matrix}\right) = \vec{u}\left(\begin{matrix} jl \\ 0 \end{matrix}\right) + \vec{u}_\lambda^p(jl), \quad (17)$$

where

$$\vec{u}_\lambda^p(jl) = -i\omega_\lambda^A \vec{u}_\lambda^p(jl). \quad (18)$$

The perturbed system with  $Q_\lambda^p(0)$  as the initial state of mode  $\lambda$  is let to evolve in a separate simulation run, as a parallel system to the original one. The initial states of all other phonon modes together with other initial conditions are exactly the same for the two parallel systems. For the same well-defined mode,  $Q_\lambda^p(0)$  also evolves according to Eq. (6) with the same oscillatory and decay rate as  $Q_\lambda(0)$ . Similar to Eq. (12), for the perturbed system, we have

$$Q_\lambda^p(t) = Q_\lambda^p(0) \exp(-i\omega_\lambda^A t) \exp(-\Gamma_\lambda t) + C_\lambda^p(t), \quad (19)$$

where the use of  $C^p$  with a superscript is to distinguish from  $C$  in the original system. Although both of them are unknown, they are different, since the evolution of the perturbed system is different. Subtracting Eq. (12) from Eq. (19) we get

$$Q_\lambda^p(t) - Q_\lambda(t) = [Q_\lambda^p(0) - Q_\lambda(0)] \exp(-i\omega_\lambda^A t) \exp(-\Gamma_\lambda t) + [C_\lambda^p(t) - C_\lambda(t)]. \quad (20)$$

During a simulation run, atomic trajectories are updated at discrete time steps and so are the normal mode coordinates calculated. We also evaluate the term involving  $C^p$  and  $C$  in a discrete form. The second term on the right-hand side of

Eq. (20) can be expanded as

$$\begin{aligned} C_\lambda^p(t_n) - C_\lambda(t_n) &= [\xi_\lambda^p(t_1) - \xi_\lambda(t_1)] \exp[(n-1)(-i\omega_\lambda^A - \Gamma_\lambda)dt] \\ &\quad + [\xi_\lambda^p(t_2) - \xi_\lambda(t_2)] \exp[(n-2)(-i\omega_\lambda^A - \Gamma_\lambda)dt] \\ &\quad \vdots \\ &\quad + [\xi_\lambda^p(t_n) - \xi_\lambda(t_n)] \exp[(n-n)(-i\omega_\lambda^A - \Gamma_\lambda)dt], \end{aligned} \quad (21)$$

where  $t_n = ndt$  means at time step  $n$  with  $dt$  being the length of one time step, and  $\xi_\lambda$  is the change in the NMC for one time step due to the newly created phonons in the original system and satisfies

$$Q_\lambda(t_n) = Q_\lambda(t_{n-1}) \exp[(-i\omega_\lambda^A - \Gamma_\lambda)dt] + \xi_\lambda(t_n). \quad (22)$$

In the same way in the perturbed system,

$$Q_\lambda^p(t_n) = Q_\lambda^p(t_{n-1}) \exp[(-i\omega_\lambda^A - \Gamma_\lambda)dt] + \xi_\lambda^p(t_n). \quad (23)$$

The NMC that describes the normal mode state at the current time step can be decomposed into two parts. The first one comes from the mode state measured at the previous time step with preserved relative phase information but decreased amplitude. This corresponds to phonons of mode  $\lambda$  being scattered into other modes. The second part,  $\xi_\lambda$  (or  $\xi_\lambda^p$ ), is from all other phonon modes in the system. This corresponds to the combined result of all anharmonic phonon processes that created new phonons into mode  $\lambda$  since last time step (after the previous NMC was measured). Because we only perturb one phonon mode  $\lambda$  and the states of all other modes are exactly the same right after perturbation,  $\xi_\lambda$  is equal to  $\xi_\lambda^p$  at  $t_1$ . So the first term on the right-hand side of Eq. (21) is always zero. But starting from the second time step, the difference,  $\chi_\lambda$ , in the perturbed system begins to propagate towards all other modes. The changes in others in turn makes  $\xi_\lambda^p$  deviate from  $\xi_\lambda$ . Although the deviation is expected to increase with further propagation of the difference, the existence of a large number of different modes greatly dilutes the effect of  $\chi_\lambda$  and its impact on the states of other modes. It may take many out-scattering and back-scattering cycles before the difference between  $\xi_\lambda^p$  and  $\xi_\lambda$  becomes perceivable. The second part of each term in Eq. (21) with the exponential decay indicates that the effects from later time steps are more prominent than those from earlier time steps. The total effect is that all terms in Eq. (21) except for the first one will be nonzero and will increase progressively from a tiny initial value. In order to keep  $C_\lambda^p(t_n) - C_\lambda(t_n)$  small, we will give a small perturbation and limit the time steps. For the time period before  $\xi_\lambda^p(t_n) - \xi_\lambda(t_n)$  gets too large and if

$$C_\lambda^p(t_n) - C_\lambda(t_n) \ll Q_\lambda^p(t_n) - Q_\lambda(t_n), \quad (24)$$

Eq. (20) may be approximated as

$$\begin{aligned} Q_\lambda^p(t) - Q_\lambda(t) &= [Q_\lambda^p(0) - Q_\lambda(0)] \exp(-i\omega_\lambda^A t) \exp(-\Gamma_\lambda t) \\ &= \chi_\lambda \exp(-i\omega_\lambda^A t) \exp(-\Gamma_\lambda t). \end{aligned} \quad (25)$$

From this result we see that the initial perturbation to the phonon mode  $\lambda$  evolves the same as that described by Eq. (6). Since the underlying phonon properties are revealed through this perturbation, we will also think of it and call it a ‘‘probe’’.

From above, the angular frequency can be straightforwardly obtained by tracking the relative phase change over time. According to Eq. (25), the phase angle of  $Q_\lambda^p(t) - Q_\lambda(t)$  is

$$\psi_\lambda^w(t) = \tan^{-1} \left[ \frac{(Q_\lambda^p)^*(t) - Q_\lambda^*(t) - Q_\lambda^p(t) + Q_\lambda(t)}{(Q_\lambda^p)^*(t) - Q_\lambda^*(t) + Q_\lambda^p(t) - Q_\lambda(t)} \right]. \quad (26)$$

However, because  $\psi_\lambda^w(t)$  is wrapped and  $-\pi \leq \psi_\lambda^w(t) < \pi$ , we need to further calculate the unwrapped phase angle  $\psi_\lambda(t)$ , which differs from  $\psi_\lambda^w(t)$  by an integer multiple of  $2\pi$ :

$$\psi_\lambda(t) = \psi_\lambda^w(t) \pm 2\pi m, \quad (27)$$

where  $m$  is an integer. After unwrapping,  $\psi_\lambda(t)$  gives a sequence that changes linearly over time without abrupt discontinuities. So that

$$\omega_\lambda^A = \frac{\psi_\lambda(t) - \psi_\lambda(0)}{t}. \quad (28)$$

The above works for all traveling modes with nonzero group velocities. Nevertheless, for the stationary modes whose phase angles do not change, we have to directly fit the time sequence of  $Q_\lambda^p(t) - Q_\lambda(t)$  to a sinusoidal function to extract  $\omega_\lambda^A$ .

Next, in order to extract the lifetime  $\tau_\lambda$ , we treat  $Q_\lambda^p(t) - Q_\lambda(t)$  in a way similar to that calculating the mode energy by taking

$$\begin{aligned} &[(Q_\lambda^p)^*(t) - Q_\lambda^*(t)][Q_\lambda^p(t) - Q_\lambda(t)] \\ &= \chi_\lambda^* \chi_\lambda \exp(-i\omega_\lambda^A t) \exp(i\omega_\lambda^A t) \exp(-2\Gamma_\lambda t) \\ &= \chi_\lambda^* \chi_\lambda \exp(-2\Gamma_\lambda t). \end{aligned} \quad (29)$$

Rearranging and using Eq. (7), we have

$$\begin{aligned} \exp(-t/\tau_\lambda) &= \exp(-2\Gamma_\lambda t) \\ &= \frac{[(Q_\lambda^p)^*(t) - Q_\lambda^*(t)][Q_\lambda^p(t) - Q_\lambda(t)]}{\chi_\lambda^* \chi_\lambda}. \end{aligned} \quad (30)$$

So far, only the potential part of the probe energy based on atomic displacements has been utilized. The same  $\tau_\lambda$  is also attainable by considering the kinetic energy from velocities. But in order to achieve the best result with minimum unwanted oscillations, we find it more desirable to track the total probe energy over time. In this way, we have

$$\exp(-t/\tau_\lambda) = \frac{2E_\lambda^{\text{Probe}}(t)}{\omega_\lambda^A \omega_\lambda^A \chi_\lambda^* \chi_\lambda + \dot{\chi}_\lambda^* \dot{\chi}_\lambda}, \quad (31)$$

where  $\dot{\chi}_\lambda = \dot{Q}_\lambda^p(0) - \dot{Q}_\lambda(0)$  is the kinetic counterpart of  $\chi_\lambda$ , and

$$\begin{aligned} 2E_\lambda^{\text{Probe}}(t) &= \omega_\lambda^A \omega_\lambda^A [(Q_\lambda^p)^*(t) - Q_\lambda^*(t)][Q_\lambda^p(t) - Q_\lambda(t)] \\ &\quad + [(\dot{Q}_\lambda^p)^*(t) - \dot{Q}_\lambda^*(t)][\dot{Q}_\lambda^p(t) - \dot{Q}_\lambda(t)]. \end{aligned} \quad (32)$$

Now we are able to extract  $\tau_\lambda$  by fitting the right-hand-side expression of Eq. (30) or Eq. (31) to an exponential decay curve.

So we have given a detailed explanation and derivation of the PT method. Its implementation procedure for MD simulation is actually quite straightforward and looks much more simplified. To probe a phonon mode  $\lambda$ , we first prepare the system to be in a desired thermal state as a reference. Then we create a parallel system by adding a small perturbation of that mode to its reference state according to Eqs. (15)–(18). In Eq. (15), the relative phase  $\varphi_\lambda^p$  can be arbitrary; for the perturbation amplitude  $A_\lambda^p$ , we recommend it to be at least three orders of magnitude smaller than the lattice parameter of the material system being investigated for a minimum impact on the probed mode. In practice, the harmonic frequency is used instead of the anharmonic one in Eq. (18) to generate the perturbation as  $\omega_\lambda^A$  is not known yet. Next, both the reference and the perturbed system are to run for the same simulation length, with both their atomic displacements and velocities dumped at the same time steps for NMC calculations. After that,  $\omega_\lambda^A$  can be obtained by either linear fitting, Eqs. (26)–(28), or sinusoidal fitting of  $Q_\lambda^p(t) - Q_\lambda(t)$ , and the mode's lifetime,  $\tau_\lambda$ , readily extracted according to Eqs. (30)–(32).

### III. RESULTS

In this section, we demonstrate the validity and unique features of our method using silicon (Si), which has been frequently adopted as a model material for studying the thermal transport properties with different methods and conditions [38–40,46]. The environment-dependent interatomic potential (EDIP) [47] is chosen for the crystalline Si studied here because reasonably good thermal conductivity results have been previously reported with this potential [24,40].

All our simulations have been performed with the classical MD code LAMMPS [48]. The velocity-Verlet integration algorithm is used with a time step of 0.001 ps, which provides enough resolution to capture the highest-frequency oscillations in our material system. A typical cubic supercell containing 4096 atoms is employed with periodic boundary conditions applied in all three directions. The lattice parameter,  $a$ , of Si we use is 0.5431 nm. To create the initial perturbation, we choose a sufficiently small amplitude  $A_\lambda^p$  of  $2 \times 10^{-5}$  for any phonon mode being probed. And the harmonic frequency and displacement vectors of each mode are calculated with the analytical lattice dynamics solver in GULP [49]. Before data collection from the NVE (constant number of atoms, volume and energy) ensemble, we have made sure that the material system is well equilibrated at the target temperature.

#### A. Validity and efficiency of the PT method for probing phonon anharmonic frequencies

We first examine the validity of the PT approach starting from the mode-wise anharmonic frequencies at a finite temperature. In Fig. 1 we show comparison of the frequency shifts of Si phonons in the [100] direction at 600 K obtained from two different methods. The NMA results are extracted from the oscillations of the autocorrelation function of the potential energy of each normal mode, and the simulation run length is 40 ps to ensure all results are fully converged. While with the PT method, the simulation is run for 0.5 ps for each

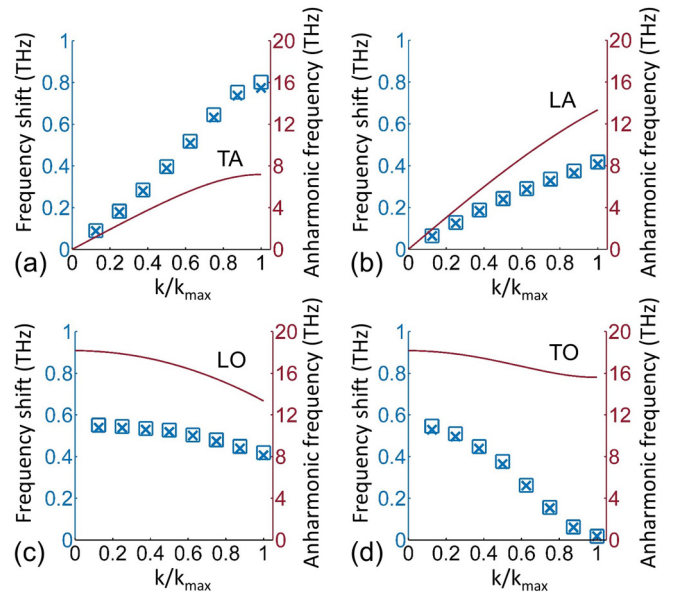


FIG. 1. Comparison of frequency shifts of Si phonons at 600 K in the [001] direction from four different polarization branches: (a) TA, (b) LA, (c) LO, and (d) TO. The NMA results are plotted as blue squares and those from the PT method are plotted as blue crosses (these correspond to the left axis). The dispersion relations are plotted as red curves (use the right axis).

individual phonon mode. The anharmonic frequency shifts are plotted as a function of reduced wave vector,  $k/k_{\max}$ , where  $k_{\max} = 2\pi/a$ , and the resulting dispersion relation of each phonon branch is also plotted in the same figure. We see that the results from the two methods agree very well. The largest difference, which is at zone boundary for the TA (transverse acoustic) branch and near zone center for the TO (transverse optical) branch, is only about 3%.

Now that the PT method is capable of revealing the delicate anharmonic frequency shifts with high accuracy, we continue to check its efficiency. In Fig. 2 we show how accurate the results the PT method provides are, as a function of simulation run length. From each different polarization branch, we sample two phonon modes, one with a relatively low and the other with a relatively high frequency. The anharmonic frequency result of each mode at a certain simulation length is obtained by fitting all previous data points directly probed during the simulation to the linear or sinusoidal function according to that described in the previous section. It is then normalized and plotted as a % of the final converged value. We see that in all cases the largest fluctuation appears in the first half phonon vibration period. The results then converge rapidly with more data points becoming available and are at more than 99% convergence by the end of one vibrational cycle.

The initial fluctuation and time needed for achieving convergence are quite mode frequency dependent. Modes with higher frequencies converge faster because fitting accuracy is proportional to how many cycles are included. In our Si case, we find that with the PT method, a simulation length of 0.3 ps is enough for a fitted frequency result with 99.5% convergence for the two low-frequency TA and LA (longitudinal acoustic) modes we sampled. For the high-frequency TA and

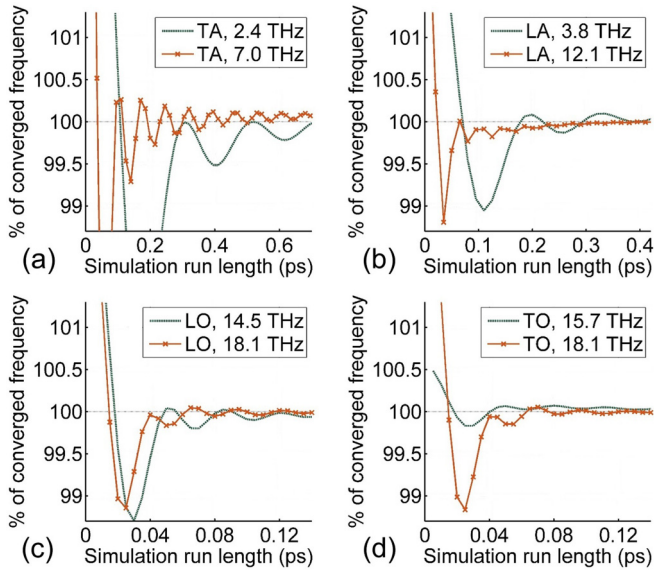


FIG. 2. Convergence of probed anharmonic frequencies with simulation run length using the PT method. Two phonon modes are sampled for each different polarization branch: (a) TA, (b) LA, (c) LO, and (d) TO.

LA modes and other modes with higher frequencies, including all LO (longitudinal optical) and TO modes, an even shorter simulation time of 0.05 to 0.1 ps is enough for very accurate results with less than 0.5% difference from the final converged value.

So we have demonstrated the validity and efficiency of our PT method for probing the anharmonic frequencies of individual phonon modes. Our focus now is on extracting mode-wise phonon lifetimes.

### B. Characteristics and validity of the PT method for probing phonon lifetimes

Some examples of the decay profiles obtained by the PT method are presented in Fig. 3, in which we have included results from three LA phonon modes with different vibrational frequencies. We see that the PT method can give us a very stable and consistent series of data points in the time period from 0 to 10 ps, which allows us to generate excellent fitting results. This is obtained right out of a single simulation run without the need to be averaged like in the statistics-based NMA method. One key benefit coming from it is that we are able to keep track of all subtle changes in the probed mode in real time, which is essential for studying the evolution of a transient process. Nevertheless, there is an error accumulation issue associated with the PT method, as we mentioned in the previous section. The smooth decay signal becomes unstable starting from 10 ps, and then abruptly changes its course. This serves as a clear sign of error eruption, meaning all data points from that moment on will be badly corrupted and shall not be included for decay fitting.

The error accumulation behavior in the PT method is more system-dependent rather than mode-dependent. Though the three phonon modes shown in Fig. 3 in our Si model have various frequencies and wavelengths, they almost experience

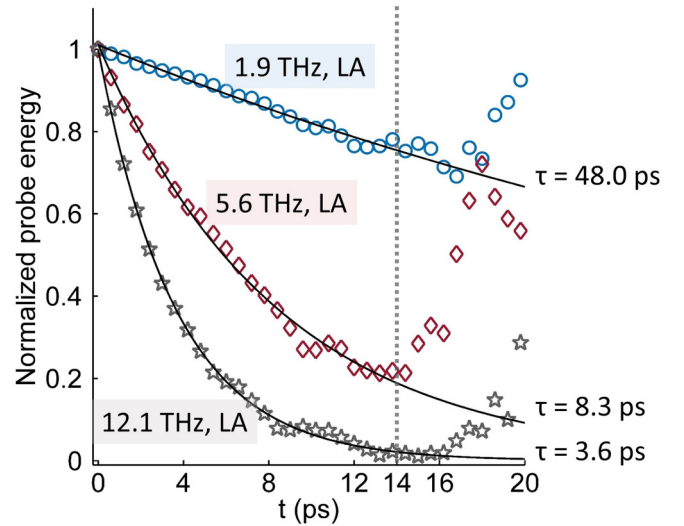


FIG. 3. Examples of the decay profiles of three LA phonon modes from the PT method. The series of discrete symbols in different colors are the total probe energy of each mode normalized by the respective initial amplitude at  $t = 0$  and each black line represents the corresponding best exponential fit.

error eruption at the same time, all about 14 ps (marked by the vertical dotted line) after creation of the initial perturbation.

Next, we plot comparison of the lifetimes of Si phonons in the [100] direction at 600 K from the two different approaches in Fig. 4. The NMA results, which have been averaged over three independent simulation runs of 1.2 ns, are plotted as

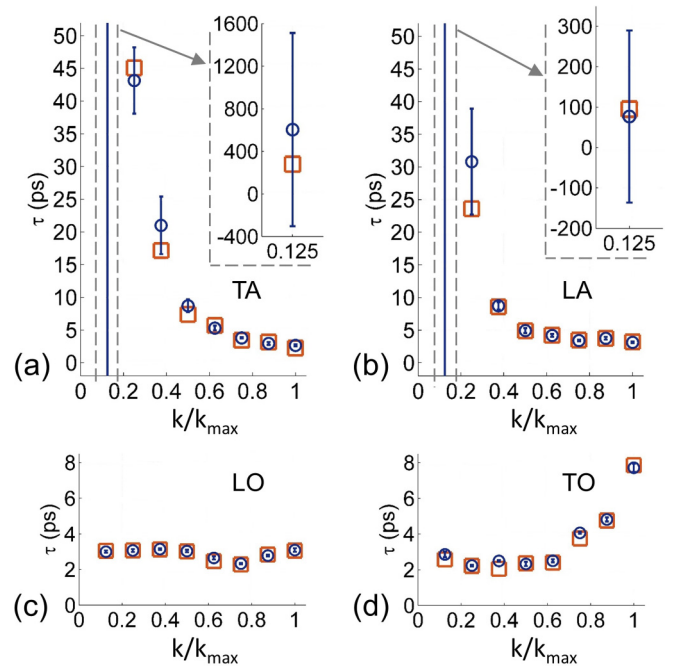


FIG. 4. Comparison of phonon lifetimes of Si in the [100] direction at 600 K obtained from the NMA (orange squares) and the PT method (blue circles with error bars). Results from four different polarization branches are presented: (a) TA, (b) LA, (c) LO, and (d) TO.

orange squares. And the PT results, each averaged over five independent short runs, are plotted as blue circles. We only include the error bars (standard deviation) from the PT method here for clarity.

We see that except for several long-wavelength (small  $k$ ) phonon modes with large  $\tau$  values, most of the results from the two methods are in excellent agreement. It is worth mentioning that neither the NMA nor the PT method distinguishes between the types of phonon scattering, such as normal, Umklapp, three-phonon or higher order processes. The lifetimes extracted here reflect the net effect from various phonon-phonon interactions and all anharmonic contributions. For short-wavelength TA modes and modes from the entire TO branch, differences in the results from the two methods are all within 15%; for short-wavelength LA modes and all modes from the LO branch, differences are only as much as 5%. The most distinguishable mismatch comes from a TA mode with a reduced wave vector of 0.125. The result from our PT method is almost twice as large as that from the NMA method. This is not unexpected given that the uncertainty extent is much larger than the mismatch itself. Because of the huge error bar, it has to be plotted separately at a different scale. Another obvious difference, coming from an LA mode with a reduced wave vector of 0.25, is about 30%. But still, it is within the coverage of the error bar. The large uncertainty mainly comes from the long lifetime of the first long-wavelength modes in the TA and LA branch. It is hard for these modes to find enough partners for anharmonic interactions and the scattering rate is unstable due to their relatively large phonon occupation fluctuations. When the wave vector becomes larger, the error bar decreases to a fairly small range, as a result of smoother and more stable decay curves. Meanwhile, we find that the entire decay profile down to near 0 like that of the 12.1 THz LA mode example plotted in Fig. 3 is not necessarily needed for an accurate fitting result. Fitting with data from a short period of time comparable to the lifetime of the probed mode is already enough to yield a reliable result with a minimal level of error. Although error bars for the NMA results are not shown here, they are actually larger than those from the PT method, even after running for hundreds of times longer simulation time. More details are provided in the following section.

### C. Accuracy and efficiency of the PT method comparing with the NMA approach for extracting mode dependent phonon lifetimes

We proceed to examine the accuracy of the results from the two methods in more depth. First, we take an LA phonon mode of intermediate frequency from Si as an example to show the convergence of lifetime results with simulation run length, which are presented in Fig. 5. The NMA result is plotted in the left panel and that from the PT method is plotted in the right panel for comparison. The average values (blue curve with symbols) and the uncertainty band (two black curves) are determined from multiple runs; we performed six independent simulation runs with the NMA approach and five runs with the PT method. It should be noted that the simulation lengths ( $x$  axis) of the two subfigures are not on the same scale. We see that the averaged NMA result gradually converges without

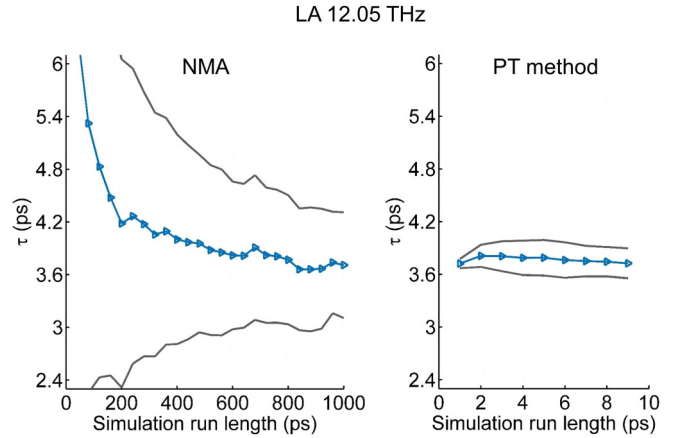


FIG. 5. Comparison of convergence of the lifetime result from the NMA approach (left) and the PT method (right) with simulation run length. Example of a Si LA mode of 12.05 THz. The blue curve with symbols in each plot is the average from multiple runs and the two black curves form an uncertainty band with its upper and lower bound being one standard deviation away from the average.

showing much variation as the simulation runs longer, and the deviation from converged value gets below 15% after 200 ps. However, the uncertainty band is quite large and is still larger than that of using the PT method even after 1000 ps of simulation time. By contrast, the PT method produces consistent results with very small uncertainty and super-short convergence time, which is less than 2 ps.

In order to have a clearer view of how accurate the lifetime results the two methods can provide and how fast they converge, we calculate the relative error (RE) as a function of simulation run length  $t$  using the following expression:

$$\text{RE}(t) = \frac{1}{\tau_{\lambda}^c} \left( \frac{1}{p-1} \sum_{i=1}^p (\tau_{\lambda,i}(t) - \tau_{\lambda}^c)^2 \right)^{1/2}, \quad (33)$$

where  $i$  indexes over  $p$  individual results from multiple runs and  $\tau_{\lambda}^c$  is the final converged lifetime of phonon mode  $\lambda$ . The calculated RE estimates the amount of variation involved in the result of one simulation run with a confidence level of about 68%, similar to that of one standard deviation calculation.

The Si results at 600 K from the two methods are plotted in Fig. 6 for comparison. From each different dispersion branch, we choose two phonon modes, one with a relatively low frequency and one with a relatively high frequency, as representatives. All of these are listed in Table I. Results of the representative acoustic modes are plotted in Fig. 6(a). From the large RE values in the left panel we see that lifetimes obtained by the NMA approach can be quite inaccurate if simulation run length and data sampling is not long enough. This is especially severe for low-frequency modes with long lifetimes. The RE values of TA-1 and LA-1 mode from 100 s run time are as high as 120%, which then slowly drop down with longer simulation length. But still, they are about 30 to 40% even after 1 ns run time. By comparison, the RE values of the same modes by the PT approach (right panel) are much smaller and decrease significantly faster. We find

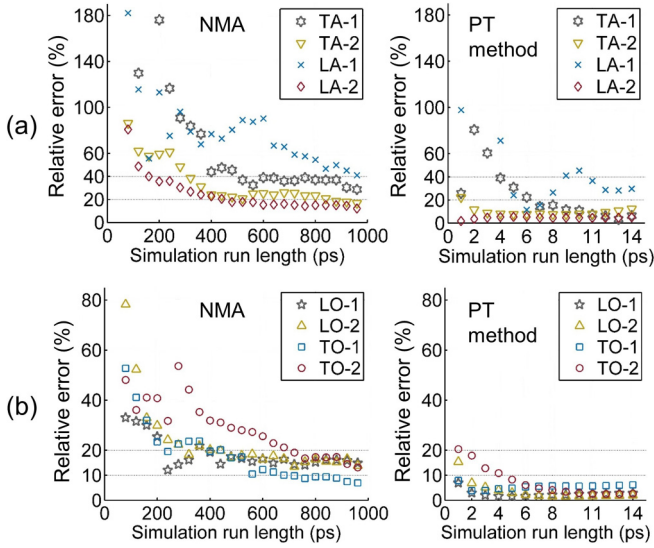


FIG. 6. Variation of the RE versus simulation run length calculated using Eq. (33) for Si phonon modes. Results from lifetimes obtained by the NMA approach are plotted in the left panel and those by the PT method are plotted in the right panel. (a) RE values for sampled TA and LA modes. (b) RE values for sampled LO and TO modes.

they are already lower than what by the NMA approach can ever achieve after only 5 ps of simulation time, and this is 200 times more efficient. The reason for this huge difference is that the NMA approach relies on averaging to cancel out the noise brought by intense thermal fluctuations, while the PT method is not based on statistics and the system-wide fluctuations are already dealt with when calculating  $Q_\lambda^p(t) - Q_\lambda(t)$ . It should be noted that the PT method does not always produce a more accurate result with longer simulation length. After certain point, the relative error starts to rebound, as can be clearly seen from the result of mode LA-1. This behavior is directly related to the nature of the method and the way postprocessing is done. We will have more detailed discussion in the next section when we further compare the PT method with the NMA approach.

For the acoustic modes with intermediate frequencies, e.g., LA-2 of Si, the errors are about one half smaller due to their shorter phonon lifetimes. The LO and TO modes with

comparably short lifetimes too have about the same level of RE, as shown in Fig. 6(b), though their vibrational frequencies are much higher. Nevertheless, a quite long simulation run is still needed for these modes to obtain converged lifetime results using the NMA approach. In the meantime, we find the level of RE and time for convergence of the results by the PT method also decrease accordingly and proportionally with the NMA results, which means the PT method is consistently more accurate and efficient.

To quantify how much more efficient the PT method is comparing with the conventional NMA approach for extracting the lifetime of a single phonon mode, we proceed to calculate the efficiency factor of using the PT method for each sampled mode. We first determine how long a simulation run time is required to achieve a RE that is below a certain level for both of the two methods. Then the efficiency factor is obtained as the ratio of the time needed by the NMA to that needed by the PT method. Five RE levels ranging from 120% to 10% are used for performance benchmarking. Results of all sampled modes from Si are tabulated in Table I. We note that because the initial RE values of mode TA-2 and LO-1 for both two methods are already below 120%, their numbers for this level are unavailable.

As can be seen in Table I, the efficiency factors for probing Si phonons are generally pretty high. The number varies depending on the accuracy level, polarization, and lifetime of a mode. For instance, the efficiency factor of mode LA-2 for achieving a RE below 120% is 1238, which means simulation time needed by the PT method is over a thousand times less than that needed by the NMA approach. This has been quite a big leap forward in performance for just a low-accuracy result. The efficiency factor keeps increasing with the result being more accurate and almost triples for a RE below 20%. After that, it becomes difficult to further improve the accuracy with the conventional NMA approach. The use of “>” sign in the last column is because the NMA result fails to converge to a RE below 10% after 1.2 ns of simulation run but the PT result achieves so in only 0.16 ps; this makes the efficiency factor on mode LA-2 greater than 7400. Similar numbers are obtained for mode LO-2, which has the same polarization as mode LA-2 and a very close frequency and lifetime. When it comes to high-frequency modes, e.g., LO-1, the NMA shows a much better performance, resulting in shorter convergence time. Thus the PT efficiency factor drops to a moderate num-

TABLE I. List of sampled modes from different polarization branches of Si and efficiency factors of using the PT method to probe phonon lifetimes at various accuracy levels.

Sampled mode	Frequency (THz)	For achieving a relative error that is below				
		120%	80%	40%	20%	10%
TA-1	2.4	580	168	128	>190	>190
TA-2	7.0	–	487	1313	704	>470
LA-1	3.8	25	156	>120	–	–
LA-2	12.1	1238	1649	1860	3851	>7400
LO-1	18.1	–	230	340	548	>2080
LO-2	14.5	1170	1580	2790	5285	>740
TO-1	18.1	1028	1146	620	1193	1289
TO-2	15.7	530	606	6672	595	>280
Average		156	203	185	498	>455



ber of around several hundred for intermediate result accuracy. We also see from the relatively low numbers with mode TA-1 and LA-1 that the PT method is less effective when dealing with low-frequency acoustic modes because of the very long lifetimes, which we have previously pointed out. In these two cases, the PT method may only provide limited reduction in computational cost by factors of tens to over a hundred for results with low to intermediate accuracy. The numbers for the remaining modes range from hundreds to several thousand. We further estimate the average efficiency factors for each accuracy level. We find an average number of about 200 is to be expected for results with low accuracy and about 500 for results with intermediate to high accuracy.

#### IV. DISCUSSION

The average efficiency factors presented in Table I are conservative estimations. Normally only one very long simulation run is performed for use with the NMA approach since information regarding all available modes has been included. But the total simulation time depends on the longest length needed by the main contributors to achieve good convergence. This total time is usually significantly longer than that required by short-lifetime modes, which means the actual efficiency factors of the PT method will be considerably higher. However, for the same reason that the NMA takes care of all modes in just one simulation run while the PT method handles individual modes in separate short runs, the overall efficiency factor, unlike the striking numbers for individual modes, is expected to be much lower. It decreases proportionally with increasing number of modes that need to be probed. Thus, the efficiency advantage of the PT method will be offset when dealing with hundreds or more modes in a system that has many dispersion branches due to complex material structure. In such situation, using the all-in-one NMA or SED analysis will be more appropriate.

The essential difference between the PT method and statistics-based methods is also seen in how the accuracy of their results changes over time. The NMA approach offers progressively more accurate results with increasing simulation length, as more data sets become available for correlation and averaging. It is worth noting that the optimal fitting length in the NMA approach is significantly shorter than the whole simulation run length. Although correlated data series can be very long, only the first short period comparable to each mode's lifetime is used to produce results with best accuracy and convergence. As for the PT method, the available fitting length is the same as simulation length. We find that the accuracy of the results using the PT method only improves in the first period of time, at the end of which the converged lifetime with lowest level of error is achieved. After that, the accuracy starts to worsen due to uncertainty from both extended fitting length and error accumulation by the method itself. Taking the acoustic mode LA-1 of Si as an example, the optimal fitting length for the best result using the PT method is about 7 ps, as is seen in Fig. 6(a) (right panel). This is far before the occurrence of error eruption, which is at 14 ps. We also notice that for a mode like LA-1 that decays slowly, the optimal fitting length of 7 ps is much shorter than its long lifetime, which is 30 ps. This shows that the PT method is well capable

of handling phonon modes with long lifetimes. Nevertheless, if the available fitting length from a single simulation run is too short and barely covers a small segment of the decay profile, there could be considerable error in the fitted result. In such a case, an average of multiple results obtained from different runs can be taken to improve the accuracy. For most of the modes that have relatively short lifetimes, the optimal fitting length is slightly longer than the lifetime of each mode.

One major superiority of the PT method is its flexibility for computationally expensive cases. Being able to efficiently probe each phonon mode separately means freedom to choose which ones we want. For a system of very large size that cannot be handled by the conventional statistical approaches, we can sparsely probe a proportion of the modes and estimate the rest by extrapolation. In some cases, when only certain modes are of interest, e.g., zone center optical modes excited by laser pulses, we can sample only those we are interested in without wasting resources on others.

There are further potential applications in which the PT method is particularly useful. For instance, studying the relaxation of a nonequilibrium system requires that the transient process is preserved. Approaches based on statistics corrupt such processes during time averaging, whereas our PT method responds to the changes and evolution in real time.

#### V. CONCLUSIONS

We have presented a PT method for probing spectral phonon properties from MD simulations. The method first creates a parallel system from the reference system by introducing a small perturbation to a normal mode of interest. The perturbation is then used as a probe to track a mode's evolution from a particular state, which oscillates and decays over time. The probe signal is obtained by comparing the normal mode states of the two systems that are running side by side. In this way, it cancels out the large noise of thermal fluctuations due to concurrent phonon-phonon processes.

Results from the PT method are benchmarked against those from the widely used NMA using EDIP Si as the model material system. We find excellent agreement on both mode-wise anharmonic frequencies and phonon lifetimes, demonstrating the validity of the method. Results are produced consistently by our method with small uncertainty and short convergence time. We find a simulation length of 0.3 ps for low-frequency acoustic or 0.05 to 0.1 ps for high-frequency acoustic and all optical modes is enough to yield a 99.5% converged anharmonic frequency in our Si case. Unlike the existing statistics-based approaches that require a very long simulation time for averaging to suppress the large noise, our method is highly efficient. We find that an average factor of about 200 to 500 reduction in computational effort is to be expected when using the PT method to extract the lifetime of a Si phonon mode with various accuracy levels. For most of the mid- to high-frequency modes (with relatively short lifetimes) we have studied, the PT method can reduce the simulation time needed by three orders of magnitude, comparing with the NMA approach. The general trend is that the efficiency advantage increases with the demand for a higher accuracy. However, our method is not suitable for handling too many

modes as the efficiency also decreases proportionally with increasing number of modes.

In the meantime, the flexibility of our method allows one to choose to probe only certain modes of interest from a large system or in a particular case. Another important feature of the method is its ability to keep track of the changes in a normal mode state in real time, which makes it ideal for studying the transient process in a nonequilibrium system. We expect the PT method to be equally well applicable to AIMD simulations, where interatomic interactions are determined from first principles. Our much higher efficiency than that of the conventional approaches can greatly ease the burden from expensive DFT-based calculations.

#### ACKNOWLEDGMENTS

This material is based upon work supported by the US Department of Energy (DOE), Office of Science, Basic

Energy Sciences, under Award No. DE-SC0006539. The work of Y.L. was supported by the US National Science Foundation (NSF) under Grant No. CMMI-1761512. X.C. was supported in part by NSF and the Louisiana Board of Regents under Award No. OIA-1541079 (CFDA No. 47.083). We would also like to thank Dr. Liming Xiong (Department of Aerospace Engineering, Iowa State University) for helpful comments. Any opinions, findings, and conclusions or recommendations expressed in this material are those of the authors and do not necessarily reflect the policies and views of DOE or NSF.

Z.Z. conceived and designed the work with inspiration from X.C. and Y.C. Z.Z. developed the methodology, ran the simulations, collected the data, and performed the analysis. Y.L. assisted in the design of this work and analysis of the results. The manuscript was written by Z.Z. with contributions from all authors.

- 
- [1] Y. Zhou, X. Gong, B. Xu, and M. Hu, *Nanoscale* **9**, 9987 (2017).  
 [2] D. G. Cahill *et al.*, *Appl. Phys. Rev.* **1**, 011305 (2014).  
 [3] E. Pop, *Nano Res.* **3**, 147 (2010).  
 [4] T. Feng and X. Ruan, *J. Nanomater.* **2014**, 206370 (2014).  
 [5] A. J. H. McGaughey, A. Jain, H.-Y. Kim, and Bo Fu, *J. Appl. Phys.* **125**, 011101 (2019).  
 [6] Y. Hu, L. Zeng, A. J. Minnich, M. S. Dresselhaus, and G. Chen, *Nat. Nanotechnol.* **10**, 701 (2015).  
 [7] A. J. Minnich, *J. Phys.: Condens. Matter* **27**, 053202 (2015).  
 [8] A. Debernardi, S. Baroni, and E. Molinari, *Phys. Rev. Lett.* **75**, 1819 (1995).  
 [9] G. Deinzer, G. Birner, and D. Strauch, *Phys. Rev. B* **67**, 144304 (2003).  
 [10] D. A. Broido, M. Malorny, G. Birner, N. Mingo, and D. A. Stewart, *Appl. Phys. Lett.* **91**, 231922 (2007).  
 [11] A. Ward, D. A. Broido, D. A. Stewart, and G. Deinzer, *Phys. Rev. B* **80**, 125203 (2009).  
 [12] L. Lindsay, *Nanoscale Microscale Thermophys. Eng.* **20**, 67 (2016).  
 [13] J. E. Turney, E. S. Landry, A. J. H. McGaughey, and C. H. Amon, *Phys. Rev. B* **79**, 064301 (2009).  
 [14] T. Tadano and S. Tsuneyuki, *Phys. Rev. B* **92**, 054301 (2015).  
 [15] T. Feng, X. Yang, and X. Ruan, *J. Appl. Phys.* **124**, 145101 (2018).  
 [16] N. K. Ravichandran and D. Broido, *Phys. Rev. B* **98**, 085205 (2018).  
 [17] F. Tian *et al.*, *Science* **361**, 582 (2018).  
 [18] P. Souvatzis, O. Eriksson, M. I. Katsnelson, and S. P. Rudin, *Phys. Rev. Lett.* **100**, 095901 (2008).  
 [19] O. Hellman, P. Steneteg, I. A. Abrikosov, and S. I. Simak, *Phys. Rev. B* **87**, 104111 (2013).  
 [20] L. T. Kong, *Comput. Phys. Commun.* **182**, 2201 (2011).  
 [21] O. Hellman and I. A. Abrikosov, *Phys. Rev. B* **88**, 144301 (2013).  
 [22] A. J. C. Ladd, B. Moran, and W. G. Hoover, *Phys. Rev. B* **34**, 5058 (1986).  
 [23] A. J. H. McGaughey and M. Kaviani, *Phys. Rev. B* **69**, 094303 (2004).  
 [24] A. S. Henry and G. Chen, *J. Comput. Theor. Nanosci.* **5**, 141 (2008).  
 [25] N. de Koker, *Phys. Rev. Lett.* **103**, 125902 (2009).  
 [26] J. A. Thomas, J. E. Turney, R. M. Iutzi, C. H. Amon, and A. J. H. McGaughey, *Phys. Rev. B* **81**, 081411(R) (2010).  
 [27] T. Lan, X. Tang, and B. Fultz, *Phys. Rev. B* **85**, 094305 (2012).  
 [28] T. Feng, B. Qiu, and X. Ruan, *J. Appl. Phys.* **117**, 195102 (2015).  
 [29] J. M. Larkin, J. E. Turney, A. D. Massicotte, C. H. Amon, and A. J. H. McGaughey, *J. Comput. Theor. Nanosci.* **11**, 249 (2014).  
 [30] H. Zaoui, P. L. Palla, F. Cleri, and E. Lampin, *Phys. Rev. B* **94**, 054304 (2016).  
 [31] E. Lampin, P. L. Palla, P.-A. Francioso, and F. Cleri, *J. Appl. Phys.* **114**, 033525 (2013).  
 [32] M. Puligheddu, F. Gygi, and G. Galli, *Phys. Rev. Mater.* **1**, 060802 (2017).  
 [33] S. G. Volz and G. Chen, *Phys. Rev. B* **61**, 2651 (2000).  
 [34] Z. Wang, S. Safarkhani, G. Lin, and X. Ruan, *Int. J. Heat Mass Transfer* **112**, 267 (2017).  
 [35] D. P. Sellan, E. S. Landry, J. E. Turney, A. J. H. McGaughey, and C. H. Amon, *Phys. Rev. B* **81**, 214305 (2010).  
 [36] R. E. Jones and D. K. Ward, *Phys. Rev. B* **97**, 054103 (2018).  
 [37] P. K. Schelling, S. R. Phillpot, and P. Keblinski, *Phys. Rev. B* **65**, 144306 (2002).  
 [38] Y. He, I. Savic, D. Donadio, and G. Galli, *Phys. Chem. Chem. Phys.* **14**, 16209 (2012).  
 [39] H. Dong, Z. Fan, L. Shi, A. Harju, and T. Ala-Nissila, *Phys. Rev. B* **97**, 094305 (2018).  
 [40] M. S. El-Genk, K. Talaat, and B. J. Cowen, *J. Appl. Phys.* **123**, 205104 (2018).  
 [41] Y. Zhou, X. Zhang, and M. Hu, *Phys. Rev. B* **92**, 195204 (2015).  
 [42] K. Säskilähti, J. Oksanen, S. Volz, and J. Tulkki, *Phys. Rev. B* **91**, 115426 (2015).  
 [43] D.-B. Zhang, T. Sun, and R. M. Wentzcovitch, *Phys. Rev. Lett.* **112**, 058501 (2014).  
 [44] G. Qin, X. Zhang, S.-Y. Yue, Z. Qin, H. Wang, Y. Han, and M. Hu, *Phys. Rev. B* **94**, 165445 (2016).

- [45] A. Cupo, D. Tristant, K. Rego, and V. Meunier, *Npj Comput. Mater.* **5**, 82 (2019).
- [46] P. C. Howell, *J. Chem. Phys.* **137**, 224111 (2012).
- [47] M. Z. Bazant, E. Kaxiras, and J. F. Justo, *Phys. Rev. B* **56**, 8542 (1997).
- [48] S. Plimpton, *J. Comput. Phys.* **117**, 1 (1995).
- [49] J. D. Gale and A. L. Rohl, *Mol. Simul.* **29**, 291 (2003).